

AFFMAE: Scalable and Efficient Vision Pretraining for Desktop Graphics Cards

David Smerkous^{*1,2} Zian (Andy) Wang^{*2,3} Behzad Najafian²

Abstract

Self-supervised pretraining has transformed computer vision by enabling data-efficient fine-tuning, yet high-resolution training typically requires server-scale infrastructure, limiting in-domain foundation model development for many research laboratories. Masked Autoencoders (MAE) reduce computation by encoding only visible tokens, but combining MAE with hierarchical downsampling architectures remains structurally challenging due to dense grid priors and mask-aware design compromises. We introduce **AFFMAE**, a masking-friendly hierarchical pretraining framework built on adaptive, off-grid token merging. By discarding masked tokens and performing dynamic merging exclusively over visible tokens, AFFMAE removes dense-grid assumptions while preserving hierarchical scalability. We developed numerically stable mixed-precision Flash-style cluster attention kernels, and mitigate sparse-stage representation collapse via deep supervision. On high-resolution electron microscopy segmentation, AFFMAE matches ViT-MAE performance at equal parameter count while reducing FLOPs by up to 7 \times , halving memory usage, and achieving faster training on a single RTX 5090. Code available at <https://github.com/najafian-lab/affmae>.

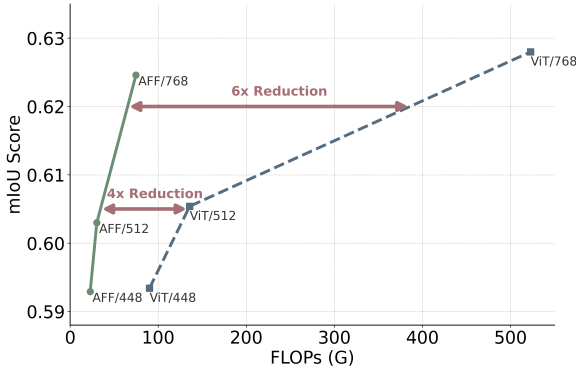


Figure 1. mIoU score on the Foot Process Width Segmentation dataset vs. Model FLOPs. Both ViT and AFF (Ours) were pre-trained MAE-style on over 170k unlabeled electron microscopy images. AFFMAE demonstrates up to a 6 \times reduction in FLOPs at high resolutions while maintaining performance comparable to the ViT baseline.

1. Introduction

Biomedical diagnostics accumulate large volumes of unlabeled high-resolution images (e.g., histology, electron microscopy, radiology), yet pretraining strong foundation models is often out of reach for many groups. Two constraints dominate in practice: (i) *compute*, since high-resolution pretraining commonly assumes server-grade multi-GPU setups, and (ii) *data governance*, where moving sensitive datasets to external cloud infrastructure can trigger lengthy HIPAA/IRB processes and institutional review. These frictions are especially pronounced in *novel* biomedical regimes—e.g., a newly studied cell phenotype, stain, scanner, or acquisition protocol—where no curated public dataset exists, but a lab may have a large private archive. In such settings, prior work repeatedly finds that pretraining on the target domain improves transfer over generic ImageNet-style initialization (Cui et al., 2018b; Mei et al., 2022; Zhou et al., 2020; 2023); more broadly, transfer improves as the pretraining distribution becomes closer to the downstream domain (Cui et al., 2018a). This motivates *in-house* pretraining methods that are feasible on desktop-class GPUs for privacy-sensitive and institutionally con-

^{*}Equal contribution ¹School of Electrical Engineering and Computer Science, Oregon State University, Corvallis USA

²Department of Laboratory Medicine and Pathology, University of Washington, Seattle USA ³Paul G. Allen School for Computer Science & Engineering, University of Washington, Seattle USA. Correspondence to: David Smerkous <smerkd@uw.edu>, Zian Wang <ziawang@uw.edu>.

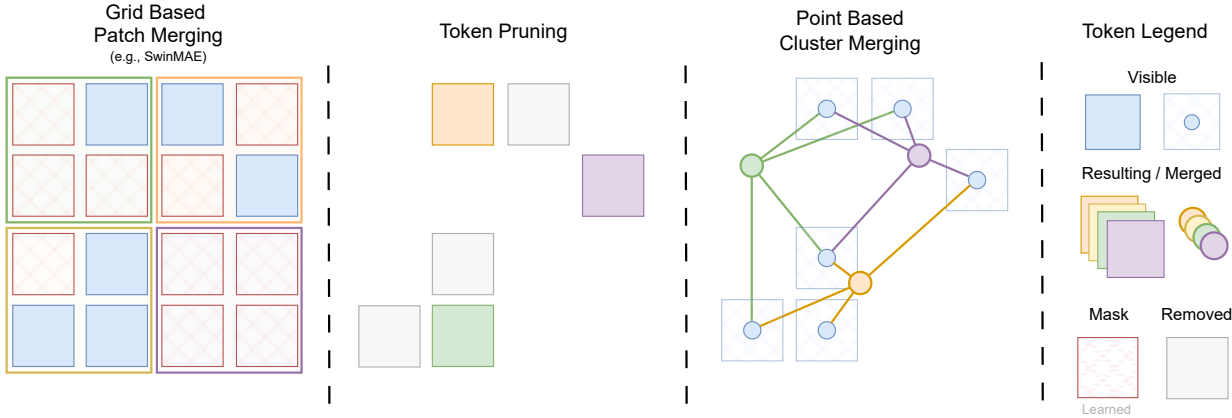


Figure 2. Three main downsampling approaches with a masked encoder. From left to right: Grid based merging: typically a patch of 4×4 tokens are merged into one output token on a grid, utilizing a learned masked token during encoding that is discarded during finetuning. We explore two novel approaches for MAE, the first being downsampling via token pruning, and a cluster point-based KNN token merging of visible tokens, both operate on visible tokens only and allow variable downsampling rates.

strained labs.

Pretraining objectives also come with different systems trade-offs. Contrastive and teacher-student approaches (e.g., CLIP, MoCo, DINO, I-JEPA) can produce strong general-purpose representations (Radford et al., 2021; He et al., 2020; Caron et al., 2021; Assran et al., 2023), but often rely on multi-view pipelines, large effective batch sizes, memory banks/queues, or teacher networks. By contrast, masked image modeling (MIM)—and in particular Masked Autoencoders (MAE)—is attractive for institutions that are privacy-sensitive, institutionally constrained, and in financially tight environments because it is unusually efficient: the encoder processes only the visible tokens and learns from a within-image reconstruction signal, avoiding cross-image mixing during training and substantially reducing activation memory and FLOPs (He et al., 2022). The same masked-modeling template has also been adapted to other targets beyond raw pixels (e.g., depth-style objectives and joint masking/reconstruction variants) (Tan et al., 2026; Bachmann et al., 2022), underscoring its continued utility as a practical pretraining method.

However, making MIM efficient at microscopy-scale resolutions requires more than choosing MAE: vanilla ViT-MAE can still be compute- and memory-intensive and slow to train on consumer GPUs. Hierarchical Transformers are a natural fit because downsampling reduces token counts, but combining *masking/token dropping* with *grid-based* hierarchies is structurally awkward. Most popular hierarchical ViTs (e.g., Swin) couple windowing, patch merging, and occasionally convolutional operations (e.g., Conv2D) to a dense lattice; when masking removes tokens, these lattice-dependent operations no longer apply cleanly and adaptations often fall back to dense bookkeep-

ing, reintroducing masked tokens, or make the encoder explicitly masking-aware, adding complexity and risking a major pretrain–finetune model mismatch, hurting downstream performance (Xu et al., 2023; Liu et al., 2023). More broadly, the rigid grid inductive bias baked into many hierarchical designs is convenient for dense prediction, but unnecessarily restrictive when the model should operate over a dynamic token set.

We address this gap with **AFFMAE**, a masking-friendly framework for *hierarchical* pretraining that is explicitly designed to make in-domain, in-house pretraining practical for consumer hardware. Building on AutoFocusFormer (Ziwen et al., 2023), AFFMAE performs adaptive, off-the-grid dynamic downsampling while keeping the encoder mask-agnostic. The key idea is to perform token merging and attention *only over the visible tokens*, preserving MIM efficiency while retaining the computational benefits of hierarchy—without architectural differences between pretraining and finetuning beyond input token masking, and focusing attention to information-rich regions. Additionally, we provide efficient Flash cluster-attention Triton kernels that run on most modern desktop GPUs, not requiring CUDA (NVIDIA et al., 2026), enabling base-model pretraining on most consumer hardware. Empirically, AFFMAE matches ViT-MAE segmentation performance at the same parameter count while using $\sim 1/10$ th of the FLOPs, $\sim 1/2$ the memory, $1.8 \times$ faster when training on an RTX 5090.

2. Related Works

Self-supervised pretraining objectives and trade-offs. Self-supervised learning for vision spans contrastive objectives (e.g., SimCLR, MoCo) (Chen et al., 2020; He

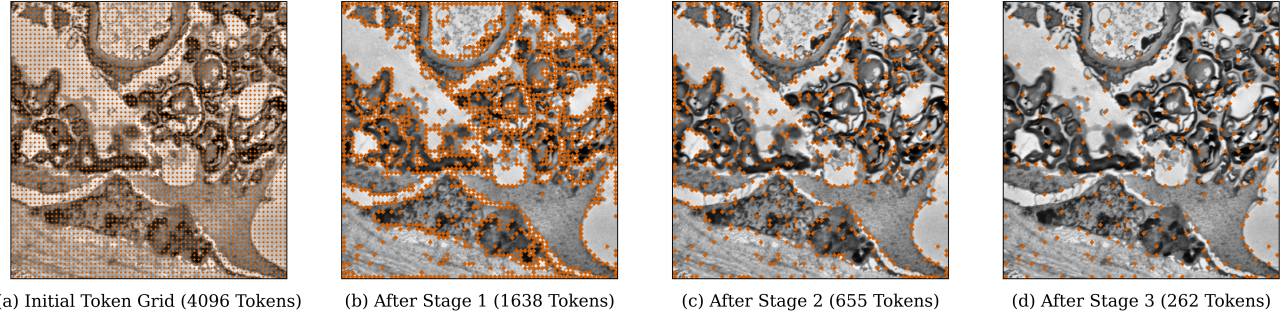


Figure 3. Visualization of adaptive token downsampling learned via AFFMAE. ($d_s = 0.4$) Starting from a dense uniform grid (a), AFF dynamically merges tokens in homogeneous regions while preserving high token density along complex structures. By the final stage (d), total token count is reduced by $\approx 94\%$.

et al., 2020), multimodal contrastive objectives (e.g., CLIP) (Radford et al., 2021), and teacher–student / self-distillation approaches (e.g., BYOL, DINO, I-JEPA) (Grill et al., 2020; Caron et al., 2021; Assran et al., 2023). These families often produce strong transferable representations, but typically rely on multi-view pipelines, large effective batch sizes (or queues/memory banks), and/or momentum teachers, which can increase memory, compute, and engineering overhead. In contrast, **masked image modeling (MIM)** methods (Bao et al., 2021; Xie et al., 2022) learn from a within-image reconstruction signal, and **Masked Autoencoders (MAE)** (He et al., 2022) are particularly appealing when compute is the primary bottleneck: MAE discards masked tokens and runs the encoder only on visible tokens, making the encoder-side cost scale with the visible token count. This efficiency makes MAE-style pretraining a practical choice for labs seeking to pretrain on private, in-domain archives using desktop-class hardware.

Hierarchical Transformers for efficient high-resolution vision. A major challenge for high-resolution imagery is that standard Vision Transformers (Dosovitskiy et al., 2020) incur quadratic attention cost in the number of tokens (Vaswani et al., 2017). Hierarchical Transformers mitigate this by progressively reducing token counts through down-sampling mechanisms such as patch merging and local attention, including Swin (Liu et al., 2021), Pyramid Vision Transformer (Wang et al., 2021), and Multiscale Vision Transformers (Fan et al., 2021). These designs substantially improve scaling to high-resolution inputs, but they typically assume a *dense, rigid lattice* of tokens to support operations such as window partitioning and grid-aligned merging.

Masked pretraining for hierarchical Transformers. Adapting MIM/MAE to hierarchical backbones is structurally non-trivial because many hierarchical operations expect dense token layouts. SimMIM (Xie et al., 2022) demonstrates that masked modeling can work well with hi-

erarchical backbones (including Swin), but it commonly retains a dense token stream with mask tokens, which differs from MAE’s core efficiency premise of *discarding* masked tokens in the encoder. SwinMAE (Xu et al., 2023) similarly must reconcile window-based computation with masking, and prior designs often reintroduce masked tokens or add encoder-side mechanisms that are specific to pretraining. MixMAE (Liu et al., 2023) proposes to replace masked tokens using visible patches from other images; while this can preserve dense structure, it introduces semantic ambiguity during hierarchical merging of tokens between different images that is not adequately addressed, multiple engineering headaches to mask attention at every stage, and is constrained by fixed masking/mixing strategies. In addition, some methods have non-reproducible results. Existing hierarchical masked-pretraining methods frequently trade off MAE’s simplicity and encoder efficiency to satisfy dense-grid requirements, and can introduce pretrain-finetune discrepancies when the encoder is made explicitly mask-aware during pretraining. Causing downstream performance to suffer as tokens seen and trained on during pretraining are no longer available during finetuning (Liu et al., 2023).

Adaptive token computation and dynamic downampling. Separately, a large body of work accelerates Transformers by adapting computation to token importance, including token pruning and dynamic inference schemes such as DynamicViT (Rao et al., 2021), A-ViT (Yin et al., 2021), and AdaViT (Meng et al., 2022). These methods typically estimate token saliency from attention or intermediate activations and prune tokens (often targeting inference-time acceleration), but there has been comparatively limited exploration of combining such adaptive, information-driven token selection with *masked pretraining* where the token set is already changing due to masking. Moreover, several dynamic schemes require careful systems design to remain compatible with automatic mixed precision and highly-optimized training kernels, especially when the token set

changes across layers. Our work builds directly toward this intersection: enabling hierarchical, adaptive downsampling under MIM-style pretraining while keeping the encoder mask-agnostic and avoiding dense-grid bookkeeping.

3. AFFMAE

3.1. AutoFocusFormer

AutoFocusFormer (AFF) (Ziwen et al., 2023) is a hierarchical backbone that replaces rigid, grid-aligned downsampling (e.g., stride-2 pooling / patch merging) with *adaptive* downsampling over an *irregular* set of token locations. Rather than defining local attention via fixed windows on a dense lattice, AFF first groups token locations into *balanced clusters* (implemented via a space-filling-curve-based procedure) to form neighborhoods of equal size to speed up knn and keep consistent token counts, and then performs local self-attention with groups of neighborhoods using relative position derived from the 2D token coordinates (Ziwen et al., 2023). After several local-attention blocks, AFF downsamples using a learnable *neighborhood merging* module: each token is assigned an importance score, and a user-specified downsampling rate $d_s \in (0, 1]$ determines how many tokens are retained for the next stage (e.g., $d_s = 0.25$ keeps 25% of tokens). The retained tokens are selected by ranking importance scores, while the remaining tokens are merged into nearby retained tokens through a differentiable, location-aware aggregation operator (point-based merging), enabling end-to-end learning of token importance (Figure 3 visualizes the results of downsampling). By operating on sets of irregularly-spaced tokens and supporting arbitrary retention ratios (rather than fixed factors like 1/2, 1/4, 1/8), AFF can focus keeping tokens in information-dense regions (e.g., small structures, Figure 3) while merging features from texture-less regions into fewer tokens (Ziwen et al., 2023).

3.2. Mixed Precision Support / Kernel Development

AutoFocusFormer (AFF) provides a strong foundation for point-based hierarchical Transformers, we found that a direct reuse of its decoder/interpolation and attention kernels can be fragile under automatic mixed precision (AMP) and can underutilize modern hardware: (i) the decoder’s inverse-distance interpolation with a *learnable* power can become numerically unstable in fp16, and (ii) the provided cluster-attention CUDA kernels materialize attention scores explicitly, limiting both speed and stability in mixed precision. We address both issues by (a) replacing inverse-power interpolation with a softmax-temperature formulation that admits numerically stable implementations, and (b) rewriting cluster attention in Triton using a FlashAttention-style streaming softmax that accumulates in fp32 while emitting fp16 outputs. In addition, we in-

roduce a point-based deformable cross-attention decoder that consumes multi-scale encoder features more effectively than using only the final-stage tokens.

Stable point interpolation with softmax. AFF’s decoder interpolates features at a query location $\mathbf{q} \in \mathbb{R}^2$ by gathering nearby tokens $\{(\mathbf{x}_i, \mathbf{f}_i)\}_{i=1}^K$ and forming a normalized inverse-distance weighted sum of the features. A typical form is

$$d_i = \|\mathbf{q} - \mathbf{x}_i\|_2 + \varepsilon, \quad \tilde{w}_i = d_i^{-p}$$

$$w_i = \frac{\tilde{w}_i}{\sum_{j=1}^K \tilde{w}_j}$$

$$\hat{\mathbf{f}}(\mathbf{q}) = \sum_{i=1}^K w_i \mathbf{f}_i,$$

where p is learnable and controls locality of weighting. In mixed precision, the inverse-power parameterization can produce extremely peaked weights (or near-zero weights) as p grows, which amplifies fp16 underflow/overflow in \tilde{w}_i and can quickly get gradients in more shallow layers.

We explored replacing the inverse-power weighting for interpolation with an exponential kernel:

$$\tilde{w}_i = \exp(-p d_i),$$

$$w_i = \frac{\exp(-p d_i)}{\sum_{j=1}^K \exp(-p d_j)} = \text{softmax}(-p d_i)$$

which is exactly a softmax with a learnable temperature ($-p$). This rewrite enables the use of standard numerically stable softmax implementations (e.g., subtracting the maximum logit) that have been proven to work, improving AMP robustness while retaining the same inductive control over locality: larger p yields sharper (more local) interpolation, smaller p yields smoother aggregation.

Point-based deformable cross-attention decoder. To better exploit multi-scale encoder features, and avoid relying solely on the final-stage tokens, we introduce a point-based deformable cross-attention decoder (Xia et al., 2022; Ziwen et al., 2023). For each decoder query token with feature \mathbf{f} and reference location $\mathbf{r} \in \mathbb{R}^2$, we predict a sampling offset

$$\Delta = g(\mathbf{f}), \quad \mathbf{q} = \mathbf{r} + \Delta, \quad (1)$$

where $g(\cdot)$ is a small linear projection. For each encoder stage ℓ , we gather the K nearest tokens to \mathbf{q} (by KNN in 2d token coordinate space) from that stage’s token set, and form a *virtual sampled token* via the temperature-softmax interpolation above:

$$\hat{\mathbf{f}}^{(\ell)}(\mathbf{q}) = \sum_{i=1}^K \text{softmax}(-p d_{\text{knn}}(q)_i) \mathbf{f}_{\text{knn}}^{(\ell)}(q)_i. \quad (2)$$

Deformable cross-attention is applied on stage-wise features, followed by deformable self-attention, in a U-Net-like fashion across encoder scales. The initial set of query tokens are a learnable mask-token with absolute positional encoding, and encoder features are encoded with absolute positioning during cross-attention. This keeps the encoder mask-token free by simply using the masked query tokens and learned interpolation on encoder tokens to form the attention mechanism. Additionally, since this is applied at each stage, the finer spatial detail during decoding can be reconstructed.

Flash-style cluster attention in Triton. Finally, the original cluster-attention implementation explicitly forms the attention matrix (e.g., computing QK^\top and storing scores before multiplying by V), which is both memory-intensive and can be numerically fragile in fp16. We re-implement local cluster attention in Triton to follow the core FlashAttention (Dao et al., 2022) principle: **stream** attention compute, fusing the neighborhood attention operations

$$\text{FlashNbhdAttn}(Q, K, V) = \text{softmax}(Q_n [K_n \ K_{\text{blank}}]^\top + B_n) [V_n \ V_{\text{blank}}]$$

without materializing the full score matrix. Where K_{blank} and V_{blank} are the neighborhood learned blank tokens, to reduce attention norms in textureless areas as described in Ziwen et al. We accumulate the softmax normalization in fp32, support relative-position bias B_n for the neighborhood, and write outputs in fp16. This improves half-precision stability since softmax attention can commonly underflow fp16; while also reducing memory traffic and improving throughput.

3.3. Deep Supervision

When adapting AFF to MAE pre-training with aggressive downsampling, we empirically observe a severe degradation in the representational quality of the deepest encoder stages. Specifically, Principal Component Analysis (PCA) visualizations of the latent tokens at the final, sparsest stages reveal a loss of semantic structure. Without intervention, the features degenerate into uniform, grid-like patterns, indicating that the tokens have collapsed and are primarily representing their positional embeddings rather than the underlying image semantics (Figure 4)

To prevent this representational collapse, we employ Deep Supervision (Lee et al., 2015) as a structural regularizer. We attach lightweight, auxiliary reconstruction heads directly to the intermediate encoder stages. By forcing the network to reconstruct the masked input directly from these intermediate tokens, we inject a strong, localized learning signal that encourages the retention of high-fidelity semantic information before the tokens undergo further aggressive merging.



Figure 4. PCA projections of the learned representations. To provide a dense spatial grid rather than a scattered set of tokens, these features are visualized after the decoder’s cross-attention. Without deep supervision (center), features collapse into homogeneous states at the deepest stage. Deep supervision (right) successfully preserves rich feature diversity at the deepest stage.

sive merging.

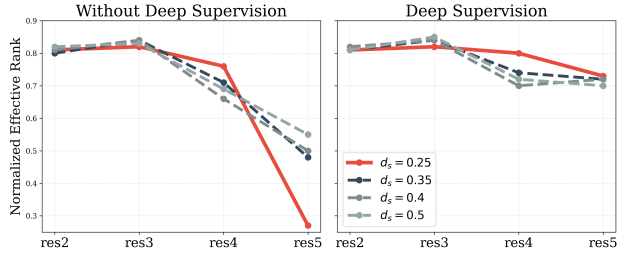


Figure 5. Normalized Effective Rank. The evolution of representation rank across layers, computed from the encoder tokens.

We validate the use of Deep Supervision by monitoring the Normalized Effective Rank (Roy & Vetterli, 2007) \hat{R} of the feature space. For a batch of tokens at a specific downsampling stage with singular values σ_i , \hat{R} is the exponential of the spectral entropy normalized by the dimension:

$$\hat{R} = \frac{1}{\min(N, D)} \exp \left(- \sum p_i \log p_i \right), \quad p_i = \frac{\sigma_i}{\sum \sigma_j} \quad (3)$$

Where N and D represent the number of tokens at that stage and the embedding dimension, respectively. Figure 5 visualizes the evolution of \hat{R} across encoder stages. We observe a clear correlation between sparsity and collapse:

- *No Deep Supervision:* As the downsampling rate becomes more aggressive, the effective rank plummets at deeper stages. This phenomenon is severe even at moderate downsampling rates.
- *With Deep Supervision:* The injection of auxiliary gradients maintains high effective rank ($\hat{R} > 0.7$) across all stages, independent of the downsampling rate.

3.4. Perlin Masking

At high resolutions, random masking becomes increasingly ineffective. As the relative patch size decreases, the model can trivially interpolate the missing information from immediate neighbors without capturing the inherent patterns of the biological structures. We therefore seek a masking

strategy that can remove continuous regions analogous to biological features. This ensures that the only way to minimize reconstruction loss is by learning global context and structural coherence, rather than relying on local interpolation between visible tokens. To achieve this, we utilize Perlin Noise (Perlin, 1985) to generate the masks (shown in Figure 6).

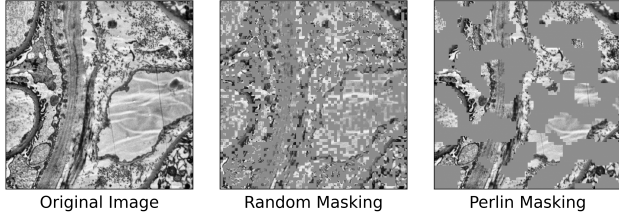


Figure 6. Illustration of our Perlin Masking strategy with a masking ratio of 0.5 and a patch size of 8.

To validate the plausibility of our masking strategy, we analyze the spectral statistics of the generated masks compared to the intrinsic statistics of the EM dataset. Natural images, including biological microscopy, exhibit a power spectral density (PSD) that follows a power law decay $S(f) \propto 1/f^\alpha$ (typically $\alpha \approx 2$) (Field, 1987; Ruderman & Bialek, 1994).

We compute the radially averaged PSD for the input images and the binary masks generated by both random and Perlin strategies. Let $M(x, y)$ be the binary mask. Its power spectrum is given by $P(u, v) = |\mathcal{F}\{M(x, y)\}|^2$, where \mathcal{F} denotes the 2D Discrete Fourier Transform. The 1D radial profile is obtained by the following:

$$PSD(f) = \frac{1}{N_f} \sum_{\mathbf{k} \in \Omega_f} P(\mathbf{k}) \quad (4)$$

Where $\Omega_f = \{(u, v) | \sqrt{u^2 + v^2} \approx f\}$ is the set of all spatial frequencies at radius f while N_f is the number of such frequencies.

Figure 7 presents the results. Specifically, we observe the following:

- The EM images exhibit the characteristic $1/f$ decay of natural signals.
- Random Masking disrupts this statistics, introducing a high-frequency plateau (white noise artifacts) and a significant spectral gap at mid to low-frequencies.
- Perlin Masking's spectral profile closely tracks the slope and magnitude of the real biological signal with barely any gaps over the entire frequency range.

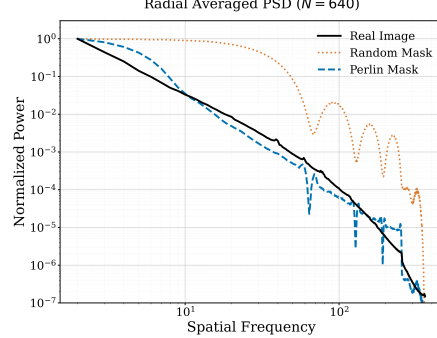


Figure 7. Spectral analysis of masking strategies. The 1D radially averaged power spectral density (PSD) is computed for real EM images, Random masks, and Perlin masks. Profiles are averaged across 640 samples and plotted on a log-log scale

4. Experiments

We evaluate our proposed framework on the task of high-resolution semantic segmentation for Electron Microscopy (EM). We first describe the experimental setup, followed by a comparison with standard ViT-based MAE baselines, ablation studies on architectural and training components, and an analysis of data efficiency.

4.1. Experimental Setup

Datasets. For self-supervised pre-training, we utilize an in-house unlabeled dataset consisting of 187,270 EM scans. For supervised fine-tuning, we use the FPW dataset, containing 570 training images and 164 test images. The segmentation task involves four semantic classes: Lamina Densa (LD), Lamina Rara Interna (LRI), Podocyte Glomerular Basement Membrane Interface (PGMI), and Foot Process Filtration Slits (Slits), alongside a background class.

Pre-training. We pre-train for 300 epochs on a single consumer-grade NVIDIA RTX 5090. Images are resized to 512×512 with a patch size of 8. We use a batch size of 64 with 4 gradient accumulations, resulting in an effective batch size of 256. We use the AdamW optimizer with $\beta_1 = 0.883$, $\beta_2 = 0.935$, and a weight decay of 0.05. The learning rate follows a cosine annealing schedule with a base of 5.0×10^{-4} and a 10,000-step linear warmup. Minimal augmentation is applied (Resize, Normalization) during pre-training.

Fine-tuning. We fine-tune end-to-end for 700 epochs at 448, 512, and 768 resolutions using the AdamW optimizer with cosine annealing learning rate schedule and 25-epoch warmup. Layer-wise Learning Rate Decay (LLRD) is applied with a factor of 0.6. To handle class imbalance, we employ a combined BCE and Dice loss, weighted by class

Table 1. Resolution Scalability. Comparison of AFF-Small ($d_s = 0.4$) vs. ViT at increasing image resolutions. Our method retains segmentation performance within 0.5% of the dense baseline while reducing FLOPs by up to $13\times$ and VRAM by $2\times$, enabling high-resolution training on consumer-grade hardware.

Model	Resolution	mIoU	FLOPs (G)	VRAM (GB)	Speed (img/s)
ViT	448	0.5934	90.08	5.74	242.9
AFF	448	0.5929	22.78	3.05	258.5
ViT	512	0.6054	135.77	7.39	166.0
AFF	512	0.6030	30.31	3.98	189.6
ViT	768	0.6280	522.88	16.22	49.2
AFF	768	0.6246	74.75	8.73	67.2

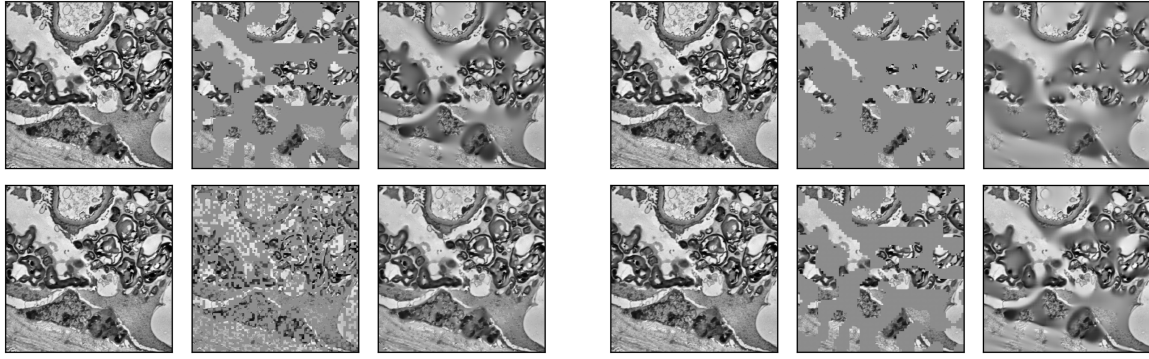


Figure 8. Reconstruction from various masking strategies. The AFFMAE model was trained with $d_s = 0.4$. Top Left: AFFMAE Perlin masking at 0.5 masking ratio. Top Right: AFFMAE Perlin masking at 0.75 masking ratio. Bottom Left: AFFMAE random masking at 0.5 masking ratio. Bottom Right: ViT Perlin masking at 0.5 masking ratio.

importance: [0.2, 2.0, 3.0, 2.0, 3.0] for Background, LD, LRI, PGMI, and Slits respectively. We employ heavy data augmentation including random flips, affine transformations, photometric distortion, and elastic transforms. Performance is reported as the mean Intersection Over Union (mIoU) on the test set.

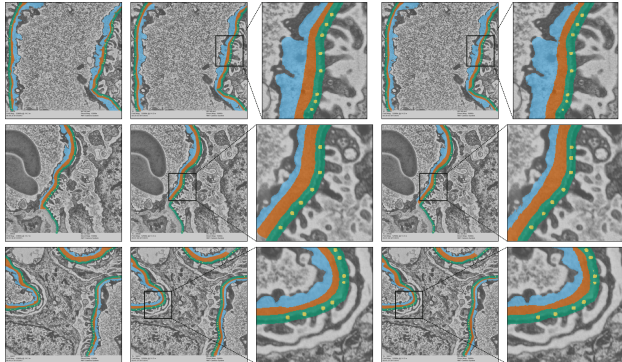


Figure 9. Qualitative segmentation results. Column 1 displays the ground-truth annotations. Columns 2 and 3 show the AFFMAE predictions and corresponding magnified insets, respectively. Columns 4 and 5 display the ViT baseline predictions with insets.

4.2. Main Results

We compare our proposed sparse pre-training framework AFFMAE against the ViT based MAE baseline across various imaging resolutions. Both models were configured to have around 22M parameters and are pre-trained for 300 epochs. For AFF, we report results at a downsampling rate of $d_s = 0.4$, which we found to offer the optimal balance of efficiency and performance. Both models utilize a lightweight decoder with embedding dimension 384, depth 4, and 6 heads. Both models utilized the same dataset, augmentations, optimizers, and Perlin masking strategy.

Reconstruction Visualizations. Figure 8 presents qualitative reconstruction results across varying masking strategies and ratios. While random masking yields smoother reconstructions, closer inspection reveals that the model primarily relies on trivial local interpolation from adjacent visible patches, predicting uniform intensities within masked areas rather than recovering textures. In contrast, Perlin masking drops contiguous regions, which forces the model to perform true spatial extrapolation. Therefore, the model can infer the underlying biological structure rather than merely propagating local pixel values. Furthermore, we observe that AFFMAE achieves a reconstruction fi

delity visually indistinguishable from the ViT baseline, despite operating on a significantly sparser token set.

Segmentation Performance. Figure 9 presents qualitative segmentation results for both the ViT and AFFMAE, fine-tuned at the 768×768 resolution. Despite operating with a significantly reduced token count due to aggressive adaptive merging ($d_s = 0.4$), AFFMAE demonstrates exceptional fidelity in capturing high-frequency, varied details, such as the podocyte filtration slits. The segmentation quality nearly identical to the ViT baseline, which relies on a computationally expensive, dense token grid. Furthermore, AFFMAE accurately segments fine-grained, low-contrast structures such as the Lamina Rara Interna. This confirms that our token merging strategy successfully preserves critical semantic boundaries without degrading downstream dense-prediction performance.

Performance vs. Efficiency. As shown in Table 1, AFFMAE maintains downstream segmentation performance comparable to ViT, for the same parameter count, while drastically reducing computational requirements. At the resolution of 512×512 , AFFMAE achieves an mIoU of 0.6030 compared to 0.6054 for the ViT based MAE, a negligible difference of 0.4%. However, this parity comes with a $4.5 \times$ reduction in Forward FLOPs (30.31G vs. 135.77G) and a 46% reduction in peak training memory (3.98 GB vs. 7.39 GB). Note that FLOPs are calculated for a forward pass on a single sample while VRAM is reported with a batch size of 16 to ensure consistency across model sizes and resolution. Figure 10 demonstrates AFFMAE’s scaling abilities visually.

Scalability to High Resolutions. The efficiency gains of our sparse architecture become increasingly pronounced at higher resolutions, where standard Vision Transformers face quadratic scaling bottlenecks. At 768×768 , the dense ViT based MAE requires 16.22 GB of VRAM, approaching the limit of high-end consumer GPUs (e.g., RTX 5080). In contrast, AFFMAE requires only 8.73 GB, fitting comfortably on mid-range hardware. Furthermore, the computational cost of the dense baseline explodes to 522.88 GFLOPs, whereas our method remains efficient at 74.75 GFLOPs, a $7 \times$ reduction.

Training Throughput. This computational efficiency translates directly to wall-clock speedups. At 768px resolution, AFF-MAE achieves a training throughput of 67.2 img/s compared to 49.2 img/s for the baseline, representing a 36% speedup, reducing the pre-training time required, which is usually the longest training stage.

Table 2. Ablation Studies.

(a) Downsampling Rate.		(b) Masking Ratio (at $d_s=0.4$).	
Rate	mIoU	Ratio	mIoU
0.50	0.6103	0.35	0.5904
0.40	0.6030	0.50	0.6030
0.35	0.5882	0.65	0.5970
0.25	0.5806	0.75	0.5974

(c) Deep Supervision (at $d_s=0.4$).		(d) Masking Strategy (at $d_s=0.5$).	
Method	mIoU	Strategy	mIoU
None	0.5903	Random	0.5926
Deep Sup	0.6030	Perlin	0.6103

4.3. Ablation Studies

We perform ablations using the AFF-Small backbone at the 512 resolution on downsampling rates, masking ratio, the addition of deep supervision, as well as the change in masking strategy.

Downsampling Rate. In Table 2a, we analyze the impact of the adaptive downsampling rate. As expected, higher token retention (0.5) yields the highest accuracy (0.6103). However, the drop-off at 0.4 is minimal, representing a sweet spot for efficiency. Aggressive downsampling (0.25) leads to a noticeable performance degradation (0.5806), likely due to the loss of fine-grained spatial details required for segmenting small structures like filtration slits.

Masking Ratio. Table 2b investigates the pre-training masking ratio. We observe that AFFMAE is robust to high masking ratios. Performance peaks at 50%, but remains strong even at 75% (0.5974). This contrasts with standard recommendation for MAE of 75%. We hypothesize this is due to the fine-grained nature of EM structures (e.g., filtration slits), where aggressive masking ($> 65\%$) breaks the connectivity of biological filaments required for the model to learn valid structural priors. All subsequent experiments use a 50% masking ratio.

Deep Supervision. We verify the necessity of Deep Supervision in sparse architectures in Table 2c. At $d_s = 0.4$, removing Deep Supervision causes a sharp performance drop to 0.5903. Re-introducing it recovers performance to 0.6030 (+2.2%). This aligns with our observation in Section 3, confirming that auxiliary losses are critical for preventing feature collapse in deep, sparse layers.

Masking Strategy. Table 2d compares standard Random masking against our Perlin masking. Random mask-

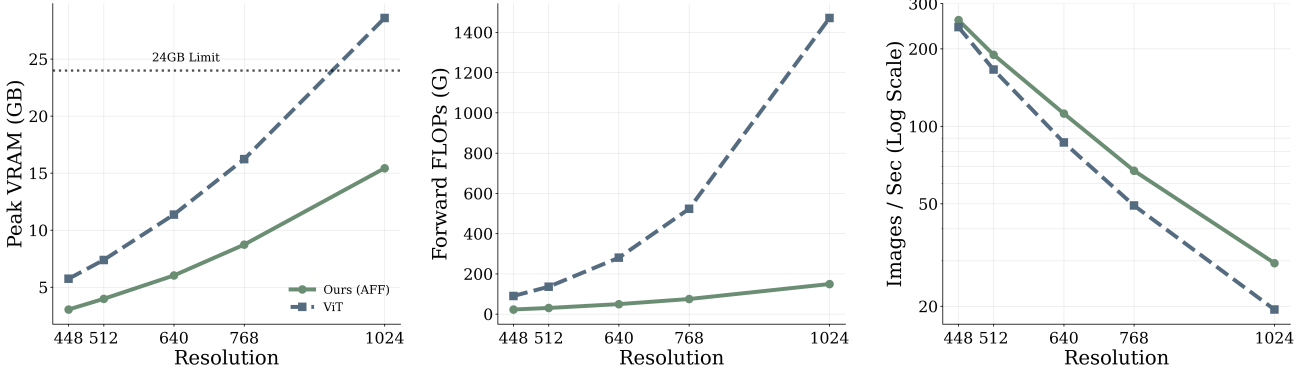


Figure 10. Computational scaling with input resolution.

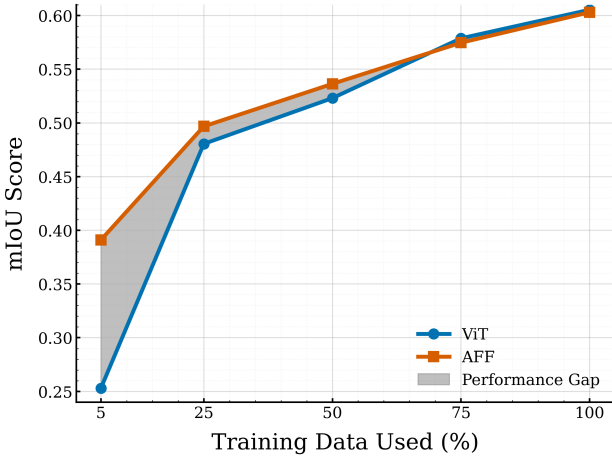


Figure 11. Fine-tuning performance of ViT and AFF as a function of available training data in percent. We observe that AFF performs much better despite having very little data to work with.

ing yields 0.5926, while Perlin masking improves this to 0.6103 (+3.0%). Random masking destroys high-frequency structural correlations that are critical for EM segmentation; Perlin noise preserves local connectivity, forcing the model to learn semantic extrapolation rather than local interpolation.

Data Efficiency. A critical constraint in medical imaging is the scarcity of annotated data. In Figure 11, we evaluate the fine-tuning performance of ViT and AFF as a function of available training data (5% to 100%). Our sparse architecture demonstrates superior data efficiency. Notably, with only 5% of the training data, AFF achieves an mIoU of 0.3910, significantly outperforming ViT (0.2529). This suggests that the priors learned by adaptive downsampling generalize better to low-data regimes.

5. Conclusion

We presented AFFMAE, a masking-friendly hierarchical pretraining framework designed to enable high-resolution self-supervised learning on consumer-grade GPUs. By combining adaptive off-grid token merging with a mask-agnostic encoder, numerically stable mixed-precision kernels, and structured masking strategies, AFFMAE preserves the efficiency benefits of MAE while inheriting the computational scalability of hierarchical Transformers.

Empirically, AFFMAE achieves up to a 7 \times reduction in FLOPs and a 2 \times reduction in memory usage compared to a ViT-MAE baseline, while matching downstream segmentation performance within 0.4% mIoU at equal parameter counts. These improvements translate directly into practical training speedups and enable high-resolution pretraining on desktop-class hardware.

Beyond 2D imaging, we believe adaptive dynamic downsampling combined with masking-aware hierarchical encoders will become increasingly important for other dense prediction tasks on higher-dimensional data (e.g., 3D or 4D imaging), where token counts grow rapidly and strictly operating on a grid drastically increases compute. We hope this work lowers the barrier to scalable in-domain pretraining and broadens access to foundation-model development in resource-constrained research environments.

Acknowledgments

We gratefully acknowledge Michael Mauer for providing and curating the majority of the electron microscopy (EM) dataset used for self-supervised pretraining. This dataset was foundational to the large-scale in-domain training experiments conducted in this study.

References

Assran, M., Duval, Q., Misra, I., Bojanowski, P., Vincent, P., Rabbat, M., LeCun, Y., and Ballas, N. Self-supervised learning from images with a joint-embedding predictive architecture. *arXiv preprint arXiv:2301.08243*, 2023.

Bachmann, R., Mizrahi, D., Atanov, A., and Zamir, A. Multimae: Multi-modal multi-task masked autoencoders. *ArXiv*, abs/2204.01678, 2022. URL <https://api.semanticscholar.org/CorpusID:247939918>.

Bao, H., Dong, L., and Wei, F. Beit: BERT pre-training of image transformers. *CoRR*, abs/2106.08254, 2021. URL <https://arxiv.org/abs/2106.08254>.

Caron, M., Touvron, H., Misra, I., Jégou, H., Mairal, J., Bojanowski, P., and Joulin, A. Emerging properties in self-supervised vision transformers. *CoRR*, abs/2104.14294, 2021. URL <https://arxiv.org/abs/2104.14294>.

Chen, T., Kornblith, S., Norouzi, M., and Hinton, G. A simple framework for contrastive learning of visual representations. In III, H. D. and Singh, A. (eds.), *Proceedings of the 37th International Conference on Machine Learning*, volume 119 of *Proceedings of Machine Learning Research*, pp. 1597–1607. PMLR, 13–18 Jul 2020. URL <https://proceedings.mlr.press/v119/chen20j.html>.

Cui, Y., Song, Y., Sun, C., Howard, A., and Belongie, S. Large scale fine-grained categorization and domain-specific transfer learning. In *Proceedings of the IEEE Conference on Computer Vision and Pattern Recognition (CVPR)*, June 2018a.

Cui, Y., Song, Y., Sun, C., Howard, A., and Belongie, S. Large scale fine-grained categorization and domain-specific transfer learning. In *Proceedings of the IEEE Conference on Computer Vision and Pattern Recognition (CVPR)*, June 2018b.

Dao, T., Fu, D. Y., Ermon, S., Rudra, A., and Ré, C. Flashattention: Fast and memory-efficient exact attention with io-awareness, 2022. URL <https://arxiv.org/abs/2205.14135>.

Dosovitskiy, A., Beyer, L., Kolesnikov, A., Weissenborn, D., Zhai, X., Unterthiner, T., Dehghani, M., Minderer, M., Heigold, G., Gelly, S., Uszkoreit, J., and Houlsby, N. An image is worth 16x16 words: Transformers for image recognition at scale. *CoRR*, abs/2010.11929, 2020. URL <https://arxiv.org/abs/2010.11929>.

Fan, H., Xiong, B., Mangalam, K., Li, Y., Yan, Z., Malik, J., and Feichtenhofer, C. Multiscale vision transformers. *CoRR*, abs/2104.11227, 2021. URL <https://arxiv.org/abs/2104.11227>.

Field, D. J. Relations between the statistics of natural images and the response properties of cortical cells. *J. Opt. Soc. Am. A*, 4(12):2379–2394, Dec 1987. doi: 10.1364/JOSAA.4.002379. URL <https://opg.optica.org/josaa/abstract.cfm?URI=josaa-4-12-2379>.

Grill, J.-B., Strub, F., Altché, F., Tallec, C., Richemond, P., Buchatskaya, E., Doersch, C., Avila Pires, B., Guo, Z., Gheshlaghi Azar, M., Piot, B., kavukcuoglu, k., Munos, R., and Valko, M. Bootstrap your own latent - a new approach to self-supervised learning. In Larochelle, H., Ranzato, M., Hadsell, R., Balcan, M., and Lin, H. (eds.), *Advances in Neural Information Processing Systems*, volume 33, pp. 21271–21284. Curran Associates, Inc., 2020. URL https://proceedings.neurips.cc/paper_files/paper/2020/file/f3ada80d5c4ee70142b17b8192b2958e-Paper.pdf.

He, K., Fan, H., Wu, Y., Xie, S., and Girshick, R. Momentum contrast for unsupervised visual representation learning. In *Proceedings of the IEEE/CVF Conference on Computer Vision and Pattern Recognition (CVPR)*, June 2020.

He, K., Chen, X., Xie, S., Li, Y., Dollár, P., and Girshick, R. Masked autoencoders are scalable vision learners. 2022 *IEEE/CVF Conference on Computer Vision and Pattern Recognition (CVPR)*, pp. 15979–15988, 2022. doi: 10.1109/CVPR52688.2022.01553.

Lee, C.-Y., Xie, S., Gallagher, P., Zhang, Z., and Tu, Z. Deeply-supervised nets. In *Artificial intelligence and statistics*, pp. 562–570. Pmlr, 2015.

Liu, J., Huang, X., Zheng, J., Liu, Y., and Li, H. Mixmae: Mixed and masked autoencoder for efficient pretraining of hierarchical vision transformers. In *Proceedings of the IEEE/CVF Conference on Computer Vision and Pattern Recognition*, pp. 6252–6261, 2023.

Liu, Z., Lin, Y., Cao, Y., Hu, H., Wei, Y., Zhang, Z., Lin, S., and Guo, B. Swin transformer: Hierarchical vision transformer using shifted windows. *CoRR*, abs/2103.14030, 2021. URL <https://arxiv.org/abs/2103.14030>.

Mei, X., Liu, Z., Robson, P. M., Marinelli, B., Huang, M., Doshi, A., Jacobi, A., Cao, C., Link, K. E., Yang, T., Wang, Y., Greenspan, H., Deyar, T., Fayad, Z. A., and

Yang, Y. RadImageNet: An open radiologic deep learning research dataset for effective transfer learning. *Radiol. Artif. Intell.*, 4(5):e210315, September 2022.

Meng, L., Li, H., Chen, B.-C., Lan, S., Wu, Z., Jiang, Y.-G., and Lim, S.-N. Adavit: Adaptive vision transformers for efficient image recognition. In *Proceedings of the IEEE/CVF Conference on Computer Vision and Pattern Recognition (CVPR)*, pp. 12309–12318, June 2022.

NVIDIA, Vingelmann, P., and Fitzek, F. H. Cuda, release: 13.1, 2026. URL <https://developer.nvidia.com/cuda-toolkit>.

Perlin, K. An image synthesizer. In *Computer Graphics*, Vol. 19, No. 3., pp. 287–296, 1985.

Radford, A., Kim, J. W., Hallacy, C., Ramesh, A., Goh, G., Agarwal, S., Sastry, G., Askell, A., Mishkin, P., Clark, J., Krueger, G., and Sutskever, I. Learning transferable visual models from natural language supervision. In Meila, M. and Zhang, T. (eds.), *Proceedings of the 38th International Conference on Machine Learning*, volume 139 of *Proceedings of Machine Learning Research*, pp. 8748–8763. PMLR, 18–24 Jul 2021. URL <https://proceedings.mlr.press/v139/radford21a.html>.

Rao, Y., Zhao, W., Liu, B., Lu, J., Zhou, J., and Hsieh, C.-J. Dynamicvit: Efficient vision transformers with dynamic token sparsification. In Ranzato, M., Beygelzimer, A., Dauphin, Y., Liang, P., and Vaughan, J. W. (eds.), *Advances in Neural Information Processing Systems*, volume 34, pp. 13937–13949. Curran Associates, Inc., 2021. URL https://proceedings.neurips.cc/paper_files/paper/2021/file/747d3443e319a22747fbb873e8b2f9f2-Paper.pdf.

Roy, O. and Vetterli, M. The effective rank: A measure of effective dimensionality. 01 2007.

Ruderman, D. L. and Bialek, W. Statistics of natural images: Scaling in the woods. *Phys. Rev. Lett.*, 73:814–817, Aug 1994. doi: 10.1103/PhysRevLett.73.814. URL <https://link.aps.org/doi/10.1103/PhysRevLett.73.814>.

Tan, B., Sun, C., Qin, X., Adai, H., Fu, Z., Zhou, T., Zhang, H., Xu, Y., Zhu, X., Shen, Y., and Xue, N. Masked depth modeling for spatial perception. 2026. URL <https://api.semanticscholar.org/CorpusID:285050163>.

Vaswani, A., Shazeer, N., Parmar, N., Uszkoreit, J., Jones, L., Gomez, A. N., Kaiser, L., and Polosukhin, I. Attention is all you need. In *Neural Information Processing Systems*, 2017. URL <https://api.semanticscholar.org/CorpusID:13756489>.

Wang, W., Xie, E., Li, X., Fan, D.-P., Song, K., Liang, D., Lu, T., Luo, P., and Shao, L. Pyramid vision transformer: A versatile backbone for dense prediction without convolutions. In *Proceedings of the IEEE/CVF International Conference on Computer Vision (ICCV)*, pp. 568–578, October 2021.

Xia, Z., Pan, X., Song, S., Li, L. E., and Huang, G. Vision transformer with deformable attention. In *Proceedings of the IEEE/CVF conference on computer vision and pattern recognition*, pp. 4794–4803, 2022.

Xie, Z., Zhang, Z., Cao, Y., Lin, Y., Bao, J., Yao, Z., Dai, Q., and Hu, H. Simmim: A simple framework for masked image modeling. In *Proceedings of the IEEE/CVF Conference on Computer Vision and Pattern Recognition (CVPR)*, pp. 9653–9663, June 2022.

Xu, Z., Dai, Y., Liu, F., Chen, W., Liu, Y., Shi, L., Liu, S., and Zhou, Y. Swin mae: Masked autoencoders for small datasets. *Computers in biology and medicine*, 161: 107037, 2023.

Yin, H., Vahdat, A., Álvarez, J. M., Mallya, A., Kautz, J., and Molchanov, P. Adavit: Adaptive tokens for efficient vision transformer. *CoRR*, abs/2112.07658, 2021. URL <https://arxiv.org/abs/2112.07658>.

Zhou, Y., Chia, M. A., Wagner, S. K., Ayhan, M. S., Williamson, D. J., Struyven, R. R., Liu, T., Xu, M., Lozano, M. G., Woodward-Court, P., Kihara, Y., Allen, N., Gallacher, J. E. J., Littlejohns, T., Aslam, T., Bishop, P., Black, G., Sergouniotis, P., Atan, D., Dick, A. D., Williams, C., Barman, S., Barrett, J. H., Mackie, S., Braithwaite, T., Carare, R. O., Ennis, S., Gibson, J., Lotery, A. J., Self, J., Chakravarthy, U., Hogg, R. E., Paterson, E., Woodside, J., Peto, T., Mckay, G., Mcguinness, B., Foster, P. J., Balaskas, K., Khawaja, A. P., Pontikos, N., Rahi, J. S., Lascaratos, G., Patel, P. J., Chan, M., Chua, S. Y. L., Day, A., Desai, P., Egan, C., Fruttiger, M., Garway-Heath, D. F., Hardcastle, A., Khaw, S. P. T., Moore, T., Sivaprasad, S., Strouthidis, N., Thomas, D., Tufail, A., Viswanathan, A. C., Dhillon, B., Macgillivray, T., Sudlow, C., Vitart, V., Doney, A., Trucco, E., Gugenheim, J. A., Morgan, J. E., Hammond, C. J., Williams, K., Hysi, P., Harding, S. P., Zheng, Y., Luben, R., Luthert, P., Sun, Z., McKibbin, M., O’Sullivan, E., Oram, R., Weedon, M., Owen, C. G., Rudnicka, A. R., Sattar, N., Steel, D., Stratton, I., Tapp, R., Yates, M. M., Petzold, A., Madhusudhan, S., Altmann, A., Lee, A. Y., Topol, E. J., Denniston, A. K.,

Alexander, D. C., Keane, P. A., and & Vision Consortium, U. B. E. A foundation model for generalizable disease detection from retinal images. *Nature*, 622(7981):156–163, Oct 2023. ISSN 1476-4687. doi: 10.1038/s41586-023-06555-x. URL <https://doi.org/10.1038/s41586-023-06555-x>.

Zhou, Z., Sodha, V., Pang, J., Gotway, M. B., and Liang, J. Models genesis. *CoRR*, abs/2004.07882, 2020. URL <https://arxiv.org/abs/2004.07882>.

Ziwen, C., Patnaik, K., Zhai, S., Wan, A., Ren, Z., Schwing, A. G., Colburn, A., and Fuxin, L. Autofocus-former: Image segmentation off the grid. In *Proceedings of the IEEE/CVF Conference on Computer Vision and Pattern Recognition*, pp. 18227–18236, 2023.